Hydro-mechanical coupling test and mesoscopic numerical simulation of sandstone with a single infilled joint

Ensayo de acoplamiento hidromecánico y simulación numérica mesoscópica de piedra arenisca con junta rellena simple

Chun Lin[1], Jin Yu[1,2], Yanyan Cai[1,2], Xu Chen[1,2] and Hengyi Kang[3]

[1] Fujian Research Center for Tunneling and Urban Underground Space Engineering, Huaqiao University, Xiamen 361021, China, bugyu0717@163.com
[2] State Key Laboratory for Geomechanics and Deep Underground Engineering, China University of Mining and Technology, Xuzhou, 221008, China
[3] Department of Civil Engineering, University of Hong Kong, Pokfulam, Hong Kong

DOI: http://dx.doi.org/10.6036/8757 | Recibido: 06/03/2018 • Evaluando: 06/03/2018 • Aceptado: 16/04/2018

RESUMEN

- Los estudios sobre el acoplamiento hidromecánico de piedra arenisca con junta prefabricada deben centrarse en las variaciones de las estructuras interiores bajo el efecto de acoplamiento hidráulico. Sin embargo, los estudios experimentales y numéricos existentes han enfatizado la mecánica macroscópica de la piedra arenisca diaclasada, y sólo unos pocos trabajos han explicado la evolución de la permeabilidad de las rocas diaclasadas desde la perspectiva de los cambios mesoestructurales. Aquí, se ha construido un modelo numérico de acoplamiento fluido-sólido de elementos discretos en la mesoescala para estudiar la mecánica de compresión triaxial y la evolución de la permeabilidad de la piedra arenisca diaclasada bajo presión osmótica desde la perspectiva mesoscópica. Este modelo se basó en un ensayo triaxial realizado sobre las propiedades mecánicas y permeabilidad de la piedra arenisca diaclasada a diferentes ángulos prefabricados. Se analizaron las leyes de influencia de un ángulo prefabricado (alpha) bajo condiciones de acoplamiento hidromecánico sobre las curvas de tensión-elongación desviadoras, el modo de fallo y la evolución de la permeabilidad de la piedra arenisca diaclasada. Los resultados muestran que durante el ensayo triaxial existe un círculo de presión con una gran superficie en la junta prefabricada, lo que indica que la junta prefabricada es altamente sensible a la presión hidráulica. La anisotropía de las partículas de enlace blando y las diferentes proporciones de fisuras por tracción y cortante bajo presión osmótica conducen a los diferentes picos de resistencia y modos de fallo de las muestras. Las microfisuras formadas por el fallo de adherencia de las partículas de piedra arenisca y la permeabilidad de la piedra arenisca diaclasada a diferentes ángulos prefabricados presentan diferentes leyes de variación con cambios coordinados en la mesoestructura y las microfisuras. Las conclusiones de la investigación pueden proporcionar referencias teóricas para los estudios sobre la mesomecánica de la piedra arenisca diaclasada bajo el comportamiento de acoplamiento hidromecánico.
- **Palabras clave:** Acoplamiento hidromecánico, Junta prefabricada, Acoplamiento fluido-sólido, Simulación numérica mesoscópica, Permeabilidad.

ABSTRACT

Studies on the hydro-mechanical coupling of sandstone with a prefabricated joint should focus on variations in interior structures under the hydraulic coupling effect. However, existing experimental and numerical studies have emphasized the macroscopic mechanics of jointed sandstone, and only a few works have explained the permeability evolution of jointed rocks from the perspective of mesostructural changes. Here, a numerical model of the fluid–solid coupling discrete element was constructed at the mesoscale to study the triaxial compression mechanics and permeability evolution of jointed sandstone under osmotic pressure from the mesoscopic perspective. This model was based on a triaxial test performed on the mechanical properties and permeability of jointed sandstone at different prefabricated angles. The influencing laws of a prefabricated angle (α) under hydro-mechanical coupling conditions on the deviatoric stress–strain curves, failure mode, and permeability evolution of jointed sandstone were analyzed. Results show that a pressure circle with a large area existed in the prefabricated joint during the triaxial test, which indicate that the prefabricated joint is highly sensitive to hydraulic pressure. The anisotropy of soft bonding particles and different tensile crack/shear crack ratios under osmotic pressure leads to the varying peak strengths and failure modes of the samples. The microcracks formed by the bond failure of sandstone particles and the permeability of jointed sandstone at different prefabricated angles exhibit different variation laws with coordinated changes in mesostructure and microcrack. Research conclusions can provide theoretical references for studies on the mesomechanics of jointed sandstone under hydro-mechanical coupling behavior.

Keywords: Hydro-mechanical coupling, Prefabricated joint, Fluid–solid coupling, Mesoscopic numerical simulation, Permeability.

INTRODUCTION

Natural rocks contain numerous joints, cracks, and discontinuous structural planes. Joints and structural planes are frequently filled with gravel, clay, and infiltration grouting [1,2]. An infilled joint is generally found in an environment with ground stress and hydraulic pressure. The seepage, squeezing, and flow of underground water in rocks with infilled joints significantly affect the mechanical properties of rocks. Many engineering practices have demonstrated that water inrush in mines and gushing water from surrounding rocks in tunnels are related to the seepage failure of rocks.

Traditional studies on seepage–stress coupling problems in rocks are based on the hypothesis that pores and crack structures are constant in rocks [3]. However, excavation disturbance will

definitely cause damages and cracks in rocks during practical engineering, These damages and cracks will not only degenerate the mechanical properties of rocks, but will also significantly influence their permeability. With the continuous increase in new research resources, numerical computation has been widely used by many scholars as an effective means to study seepage–stress coupling problems. To conveniently analyze the seepage–stress coupling effect of rocks, many scholars have sought for a constitutive model that can describe the seepage–stress coupling effect of rocks and have proposed various models, such as the continuous medium model of seepage [4], fracture network model of seepage [5], and double porosity model of flow [6]. The mechanical properties and permeability evolution of rocks under the seepage–stress coupling effect have been analyzed based on these models. The results of such analyses have played an indispensable role in further exploring the seepage–stress coupling effect of rocks. However, these constitutive models require considerable computational workload. Moreover, they cannot describe permeability evolution at a specific position in rocks in the finite element simulation of the stress–strain curve and the permeability curve with axial strain under the seepage–stress coupling effect of rocks. These constitutive models are difficult to apply extensively in practical engineering. They also neglect the influence of joints on the anisotropy of the seepage–stress coupling effect of rocks. Thus, existing research methodologies are inapplicable to discussing the seepage–stress coupling problems in jointed rocks.

Here, a numerical model of a jointed rock under the hydro-mechanical coupling effect was constructed using the discrete element software PFC^{2D}. This model laid the foundation for further research on the mesomechanics of jointed rocks under the fluid–solid coupling effect. The mechanical properties of rocks and the rule for permeability changes in rocks with an infilled joint should be investigated to acquire recommendations for reasonable seepage control, geological environment protection, and rock engineering safety evaluation.

2. STATE OF THE ART

Jointed rocks are widely distributed rock structures in the natural environment. Considerable research progresses on the compression and penetration mechanics of jointed rocks have been achieved. Most related works are experimental studies that have mainly focused on the effects of confining pressure and osmotic pressure on the triaxial mechanics of the compression and penetration of jointed rocks. Wong et al. [7] discussed the effects of confining pressure on the permeability of jointed rocks in a triaxial test on the mechanical properties and permeability of rock specimens using the steady-state water flow method. They concluded that the permeability of jointed rocks decreased with an increase in confining pressure. Wang et al. [8] conducted a triaxial test on the mechanical properties and permeability of sandstone under different osmotic pressure values. They reported the relationship of volumetric strain to permeability and osmotic pressure during rock deformation and failure processes. Zhang et al. [9] performed a triaxial test on the mechanical properties and permeability of jointed rocks within a confining pressure range of 1.0–3.5 MPa They then discussed the flow mechanism of water in joints and cracks and the permeability characteristics of rocks based on the results of this test. Wang et al. [10] conducted a triaxial compression test on limestone under hydro-mechanical coupling conditions based on the MTS815 mechanical testing system of rocks. The differences in mechanical properties, permeability, and relationship of peak intensity to deformation and hydraulic pressure before and after rock failure were determined. However, none of these studies has discussed the seepage–stress coupling problem in jointed rocks based on the anisotropy of joints. Consequently, they failed to interpret the influences of joint anisotropy on the failure mode and permeability evolution of jointed rocks under seepage–stress coupling conditions. Wasantha et al. [11,12] discussed the influence of joint orientation on the hydro-coupling characteristics of jointed sandstone in a triaxial test under undrained condition. They determined that the failure mechanism of jointed sandstone was mainly affected by joint orientation and confining pressure. Maximum pore–water pressure developed early in intact sandstone. However, these aforementioned researchers reported only the mechanical properties and permeability characteristics of jointed rocks under seepage–stress coupling conditions at the macroscopic level. They neither acquired data on the mesostructural changes in rocks and the microcrack initiation and propagation mechanism in jointed rocks nor explained the compression mechanics and permeability changes at the mesoscale of jointed rocks under hydro-mechanical coupling conditions. To determine the triaxial compression mechanics and permeability characteristics of jointed rocks, the sensitivity of the mechanical properties and permeability evolution of these rocks to mesostructural changes is further analyzed by investigating macroscopic mechanics. Such investigation facilitates a comprehensive analysis of the influencing factors of the compression and penetration characteristics of jointed sandstone.

In addition, many scholars have discussed the seepage characteristics of jointed rocks through numerical simulation. In particular, considerable research progresses on the hydraulic fracturing process and hydrofracture propagation of jointed rocks have been achieved worldwide. Li et al. [13] constructed an RFPA^{3D} finite element model that considered the coupled effects of seepage, damage, and stress field based on a 2D version of a finite element model. They also conducted a numerical simulation of the hydraulic fracturing process of rock samples. Shimizu et al. [14] performed a numerical simulation of fluid–solid coupling in the hydraulic fracturing process of rocks based on the discrete element software DEM. They then discussed the effects of fluid viscosity and particle size distribution on the hydraulic fracturing process. Wang et al. [15] established a seepage coupling analytical model based on FLAC^{3D} and simulated the crack initiation, crack propagation, and failure processes of jointed rocks under hydro-mechanical coupling conditions through dynamic damage and stress–strain curve analyses. Li et al. [16] proposed a numerical simulation method that considered the coupled effect of fluid flow and stress field on layered rocks by conducting numerical studies. They found that hydrofracture propagation was mainly controlled by in situ stresses, interface properties, and lithology. Marina et al. [17] conducted a numerical simulation of the fluid–solid coupling effect of a fractured limestone sample using discrete element software. They discussed the influences of fluid flow on stress state and hydraulic fracture initiation and propagation within the limestone sample. Although these studies have enhanced the understanding of the evolutionary rule for the seepage–stress coupling of jointed rocks, they barely discussed the variation laws for rock strength and permeability in the penetration process. Therefore, they cannot reflect the degradation of the mechanical properties and permeability change characteristics of jointed rocks in the hydrofracture process. Research conclusions are inapplicable to studies on the mechanical properties and permeability evolution of jointed rocks under the seepage–stress coupling ef-

fect. In accordance with fluid–solid coupling theory, Yang et al. [18] presented the relationship between the size effect and macroscopic permeability of jointed rocks under biaxial compression via a numerical method. They also discussed the sensitivity of rock strength and permeability to the size effect. The crack structure of rocks at the mesoscale is dynamic during the compression process. The development of a microcrack at the mesoscale will definitely degrade the mechanical properties and change the permeability of jointed rocks. Studies on the sensitivity of rock strength and macroporosity to the size effect have not obtained an explanation for the damage mechanism and permeability change of jointed rocks at the mesoscale caused by microcrack interaction. The influence of crack structural changes at the mesoscale on the permeability change characteristics of rocks is difficult to elaborate, and a prognosis on the permeability change characteristics of jointed rocks from the evolution of the mesostructure cannot be made.

To address these problems, a numerical model of a laboratory test was constructed using the particle flow software PFC^{2D} based on a triaxial test on the mechanical properties and permeability of jointed sandstone under different prefabricated angles. A mesonumerical simulation of the fluid–solid coupling effect was conducted in the aforementioned simulation mode to discuss the curve of the deviatoric stress with the axial strain, failure mode, and permeability evolution of jointed sandstone under osmotic pressure–stress coupling conditions. Consequently, the general rule was established. The research conclusions laid the foundation for further numerical analyses of jointed rocks.

The remainder of this study is organized as follows. Section 3 introduces the triaxial compression test under a hydro-mechanical coupling condition and the discrete element modeling approach. Section 4 analyzes the experimental and numerical results, such as the curve of the deviatoric stress with axial strain, failure mode, initial permeability characteristics, and permeability evolution. The influence of the prefabricated angle (α) on the curve of the deviatoric stress with axial strain, failure mode, and evolutionary characteristics of permeability is discussed. The validity of the discrete element model is also verified. Section 5 summarizes the conclusions.

3. METHODOLOGY

3.1. TRIAXIAL TEST UNDER HYDRO-MECHANICAL COUPLING

This study used uniform-texture sandstone without evident cracks as the experimental sample. Cylindrical specimens with a diameter of 25 mm and a height of 50 mm were collected and cut at dip angles of 0°, 30°, 45°, 60°, and 90° along the axis of the specimen. Cracks were filled with gypsum slurry. A sandstone sample with a single infilled joint is shown in Fig. 1(see section: supplementary material). In the experiment, the confining pressure was increased to 20 MPa via oil charging and axial stress was controlled via displacement. The confining pressure was kept constant. The seepage valve of the experimental apparatus was opened in the beginning of loading. A hydraulic seepage pressure of 5 MPa was applied to the upper end of the sandstone specimen, whereas the lower end of the sandstone specimen was exposed to the atmosphere. An osmotic pressure gradient was formed along the axial direction of the specimen, which was conducive to realizing the triaxial test on the mechanical properties and permeability of jointed sandstone [19]. The results demonstrate that the peak strength of the stress–strain curve increases with an increase in the prefabricated angle (α), whereas peak strain initially increases and then decreases until it reaches the maximum value (α=60°). The experimental results were introduced into the follow-up numerical simulation analysis. Parameter calibration in the discrete element model was based on the curve of the deviatoric stress with axial strain. Such calibration aimed to realize the response of the mechanical properties and hydraulic characteristics reflected in the numerical model and the actual experiment.

3.2. A DISCRETE ELEMENT MODEL AND DETERMINATION OF MESOSCOPIC PARAMETERS

3.2.1 The fluid–solid coupled equation of particle flow

In accordance with fluid–solid coupling theory of particle flow, the closed fluid domain formed by the contact bond of adjacent particles provides a space for fluid flow, whereas bond rupture between particles offers seepage channels for the fluid. The algorithm is shown in Fig. 2(see section: supplementary material).

In the model, the fluid forms a laminar flow in the channels and the volumetric rate of flow conforms to the cubic law:

$$Q = \frac{a^3}{12\mu}\frac{(P_2 - P_1)}{L} \tag{1}$$

where μ (Pa·s) is fluid viscosity; (P_2-P_1)(N) and a (m) stand for pressure difference between adjacent fluid domains and the width of channel, respectively; L is the length of channel.

In the calculation, L takes the sum of the radius of adjacent particles:

$$L = \frac{4r_1 r_2}{r_1 + r_2} \tag{2}$$

When the initial width of the channel (a_0) is given, the width of the channel (a) is calculated using the following formula relative to normal pressure (F) on the bond of particles:

$$a = \frac{a_0 F_0}{F + F_0} \tag{3}$$

where F_0 (N) is the normal pressure when the width of channel is reduced to half of the initial width, and F (N) is the normal pressure under current load.

Fluid pressure, which is accumulated in the fluid domain, is shown in Fig. 3(see section: supplementary material). The resultant force (F_d) produced by fluid pressure (P) on particles with a radius of r is expressed as:

$$F_d = \int_{-\beta}^{\beta} P\cos\theta r d\theta = P\mathbf{n}_i s \tag{4}$$

where β(°) is half-angle of fluid boundary, s(m) is the width of the fluid pressure, and n_i is direction vector.

3.2.2 Numerical model of jointed rock mass

In the current study, the size of the particle flow model was set as 25 mm × 50 mm. Cheng et al. [20] concluded that particles piled up from top to bottom, and the numerical model was generated via repeated falling and stacking. Particles in the infilled joint were relatively loose and exhibited high porosity. The prefabricated joint and non-prefabricated area adopted different particle sizes and porosities. Particle size and porosity for the prefabricated joint were 0.09–0.14 mm and 0.09, respectively. Particle size and porosity for the non-prefabricated area were 0.3–0.45 mm and 0.07, respectively. Finally, 3,014 particles were generated. The

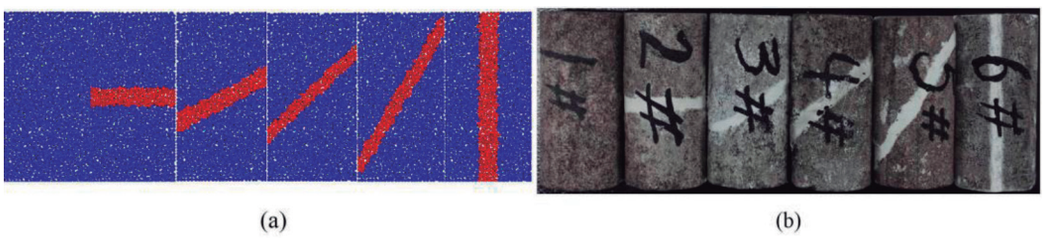

Fig. 4. The intact sample and the samples with a single infilled joint. (a) The PFC numerical models of the intact sample and the samples with a single infilled joint.(b) The physical images of the intact sample and the samples with a single infilled joint

bond model was a parallel bond model. The intact sample and the samples with a single infilled joint are shown in Fig. 4.

The principle of the hydro-mechanical coupling test and the initial conditions for the simulation are presented in Fig. 5. A constant loading of P_2=20 MPa was applied to the numerical model by implementing the servo command. Then, P_3=5 MPa was applied to the top of the model. Before loading, 0.1 MPa was exerted to the fluid domain of particles to indicate the saturated rock masses in the experiment and achieve an osmotic pressure difference of approximately 5 MPa. P_1 was applied as the axial stress at a step rate of 0.01 mm/10^4 until the specimens ultimately failed. Pore–water pressure penetrated continuously downward during the loading process. The simulated seepage process is illustrated in Fig. 6 (α=45°). Seepage flow in the fluid domain was stable at 30,000 steps. Large and dense pressure circles were formed in the fluid domain at the prefabricated joint, and the accumulative pore–water pressure in the pressure circles was considerable. Therefore, pore–water pressure at the prefabricated joint was higher than that at the non-prefabricated area.

3.2.3 Determining the mesoscopic parameters

The trial-and-error method was applied to calibrate the mesoparameters. The mesoparameters were repeatedly calibrated to determine their responses and the macroscopic mechanics of the materials in the model. In accordance with the results of Wang et al. [21], hydraulic parameters were inputted into the selected model to compute hydro-mechanical coupling under osmotic pressure. The modulus of elasticity and peak strength in the curve of the deviatoric stress with axial strain were close to the experimental results obtained through the repeated calibration of parameters, which aimed to verify the reasonability of the mesomechanical parameters. The mesoparameters and the calculation parameters of the fluid are shown in Tables I and II (see section: supplementary material).

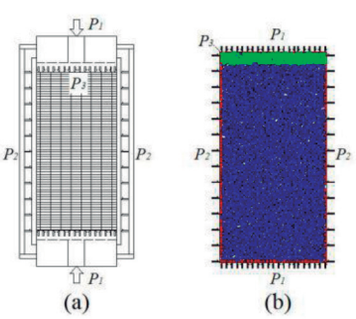

Fig. 5. Hydro-mechanical coupling test and the initial conditions of simulation. (a) The principle of the hydro-mechanical coupling test.(b) The initial conditions for the simulation

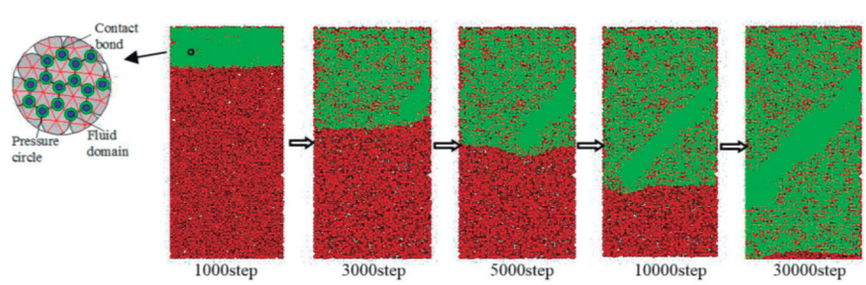

Fig. 6. Simulated seepage process at the prefabricated angle of 45°

4. DISCUSSION

4.1. EFFECT OF JOINT ANGLE ON THE DEVIATORIC STRESS–STRAIN CURVES OF ROCK SPECIMENS

The numerical computational and experimental results of the deviatoric stress–strain curves of sandstone with infilled joints are presented in Fig. 7. The numerical computational and literature results [19] are compared in Table III (see section: supplementary material). Numerical calculations of peak strength and peak strain are roughly similar to the overall trend of the literature data. As Fig. 7 and Table 3 show, the peak strain increases firstly and then decreases with the increase of the prefabricated angle, and the maximum value is obtained at the prefabricated angle of 60°. The peak strengths of the specimens are proportional to the prefabricated angle. The peak strength of intact sandstone is close to that at the prefabricated angle of 90°. The maximum peak strength (approximately 76.81 MPa) is achieved at a prefabricated angle of 90°. This value is approximately 25.8 MPa higher than the minimum peak strength (at a prefabricated angle of 0°). In accordance with contact force theory of adhesive spherical particles [22], the interaction force of particle clearance between two surfaces (h_0) is F:

$$F = \frac{2}{3}\left[4\left(\frac{\varepsilon}{h_0}\right)^2 - \left(\frac{\varepsilon}{h_0}\right)^8\right]\pi R^* \triangle \mathrm{r} \tag{5}$$

$$\frac{1}{R^*} = \frac{1}{R_1} + \frac{1}{R_2} \tag{6}$$

where ε(m) is equilibrium spacing of particle, h_0(m) is the particle clearance, Δr(J) is bonding energy , and R^*(m) is the effective particle radius.

As Equation (5) shows, the contact adhesive force of particles is inversely proportional and highly sensitive to the equilibrium spacing of particles [23]. When an infilled joint is distributed along the axial direction, its porosity is high. The equilibrium spacing of particles (ε) is large, whereas the axial stress of particles (F) is minimal. The bond strength of particles at the prefabricated joint is low. By contrast, when the infilled joint is distributed along the horizontal direction, the axial component of the equilibrium spacing of particles (ε) decreases and the bond strength of particles at the prefabricated joint increases accordingly. Bond

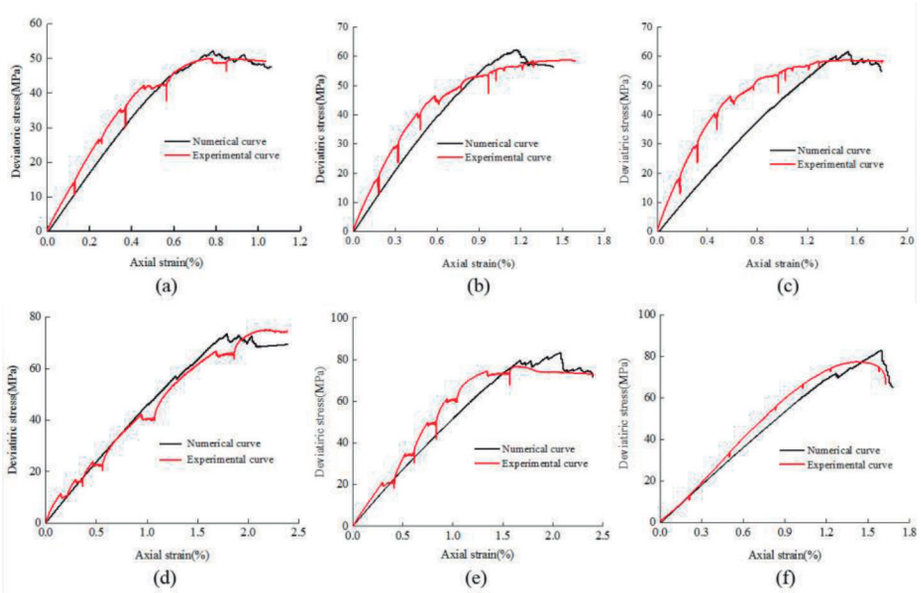

Fig. 7. Relation curves of the experimental stress and numerical stress with axial strain at different prefabricated angles (a) α=0°.(b) α=30°.(c) α=45°.(d) α=60°.(e) α=90°.(f) Intact sample

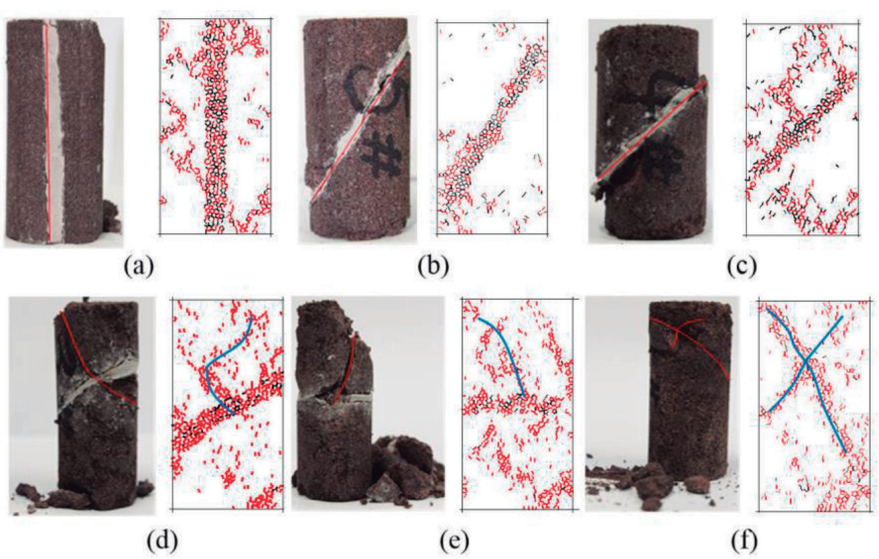

Fig. 8. The pattern of sandstone sample failure mode and simulated failure mode (a) α=0°.(b) α=30°.(c) α=45°. (d) α=60°.(e) α=90°.(f) Intact sample

strength increases as the prefabricated angle increases, and the peak strength of the curve of the deviatoric stress with axial strain increases significantly. Therefore, the peak strength of the specimens is proportional to the prefabricated angle, whereas the peak strain presents an inverted V-shaped variation with an increase in the prefabricated angle, which reaches its peak at α=60°. After water saturation, osmotic pressure in the jointed rocks propagates through the fluid domain and then transmits to the particles. The porosity and area of the fluid domain at the prefabricated joint are high. Under osmotic pressure, the equilibrium spacing of jointed particles decreases and the bond strength of particles is enhanced, thereby increasing the condensation degree of particles. Consequently, the bond strength of the sandstone specimens with infilled joint fluctuates during the post-peak stage. On the curve of the deviatoric stress with axial strain, the deviatoric stress is kept stable within a certain period during the post-peak stage, which is mainly manifested by an up-and-down oscillation phenomenon. No weak infilled joint is found in the intact sandstone specimen. The deviatoric stress during the post-peak stage of the sandstone specimen decreased sharply under hydro-mechanical coupling conditions, thereby resulting in brittle failure. This finding indicates that the infilled joint can keep the deviatoric stress stable within a certain period during the post-peak stage under hydro-mechanical coupling condition.

4.2. THE FAILURE MODE

The simulated failure mode and the failure mode of literature [19] are shown in Fig. 8. The failure area and failure mode of rock specimen are generally similar to those in the literature pattern. When particles bear excessive normal force or shear force, their bonds are destroyed and two types of cracks are generated: tensile cracks (red) and shear cracks (black). When the prefabricated angle is large (i.e., α=60° or 90°), the bonds of the particles at the prefabricated joints are destroyed, and numerous tensile cracks and a few shear cracks are generated. The tensile cracks at the prefabricated joint comprise a high proportion of cracks. Tensile cracks nucleate on the large scale and run through the prefabricated joint band. Several shear cracks are accompanied randomly by non-prefabricated joints. When the prefabricated angle is small (i.e., α=30° or 45°), large-scale nucleation of shear cracks occurs at the prefabricated joint and few tensile cracks are formed among shear cracks. Numerous microcrack nucleations develop at the top or bottom of the non-prefabricated area. The numbers of tensile and shear cracks are generally equal. The nucleations of shear cracks are abundant, and shear cracks run through the prefabricated joint band. When α=0°, the nucleations of tensile and shear cracks at the prefabricated joints, which run through the joint band of the sandstone specimens, are considerable. The proportions of tensile and shear cracks are equal. No evident distribution pattern of microcracks is formed at the non-fabricated joints. The nucleations of tensile cracks are abundant in the intact sandstone specimen and are distributed in a crossing pattern surrounded by few microcracks. The failure modes of the specimens at different prefabricated angles are divided into several types according to the failure mode of jointed sandstone and the distribution law of cracks. When α=0°, the prefabricated joint runs through the specimens along the axial direction and nucleations of abundant tensile and shear cracks are formed during the loading process. The specimen exhibits splitting along the prefabricated joint plane. When α=30° and 45°, numerous nucleations of abundant shear cracks are formed at the prefabricated joint. Bond rupture occurs around the prefabricated joint and is distributed along the prefabricated joint band. The specimen exhibits sliding failure along the prefabricated joint plane. When α=60° and 90°, nucleations of abundant tensile cracks are formed at the prefabricated joints and the specimens exhibit shearing across the prefabricated joint plane. The bond

ruptures of particles in the intact specimen are mainly dominated by tensile cracks, which demonstrate crossing shear failure.

4.3. SALIENT FEATURES OF INITIAL PERMEABILITY

The permeability of the specimens was monitored using the steady-state water flow method. If the seepage conforms to Darcy's law, then the permeability (k) is calculated according to seepage quantity:

$$\mathrm{k} = \frac{Q\mu L}{\Delta P A} \tag{7}$$

where L (m) and A (m^2) stand for the height and cross-section of the rock samples, respectively, and Δp (Pa) is the pressure gradient between the end-faces of the rock cores.

The permeability of the sandstone specimens (k) is estimated according to the relationship between permeability and porosity in the capillary bundle model, i.e., the Kozeny–Carman equation [24], which is presented as follows:

$$\mathrm{k} = \mathrm{c}\frac{d_p{}^2\varphi^3}{(1-\varphi)^2} \tag{8}$$

where φ is the mean porosity , d_p (m) is the mean particle-size, and the constant c, which is related to pore shape and pore connectivity has an empirical range of 0.002–0.0045. In this study, the empirical range was set as 0.002.

The permeability of sandstone during the initial state and at different prefabricated angles was calculated using Equation (7) based on the statistics of triaxial test data on seepage quantity. In a sandstone specimen, 1,250 measurement circles with a radius of 0.5 mm were placed uniformly at vertical and horizontal intervals of 1 mm. Local porosity was monitored through the measurement circles and outputted in sheets. Mean porosity (φ) was calculated based on the results. The permeability of jointed sandstone (k) was obtained when φ was substituted into Equation (8). The experimental and numerical values of the initial porosity at different prefabricated angles are shown in Fig. 9. When α=0°, the initial permeability reaches the maximum value (approximately 9.0x10^{-14} m^2), which is approximately 8.0x10^{-14} m^2 higher than the minimum value when α=90°. The initial permeability is reduced slightly when α=45°, 60°, and 90°. The decrement of the initial permeability when α=45°, 60°, and 90° is significantly lower than that when α=30°. In summary, the initial permeability of the jointed sandstone decreases significantly with an increase in the prefabricated angle.

4.4. EVOLUTIONARY FEATURES OF PERMEABILITY

The experimental and numerical permeability–strain curves of the sandstone specimens at different prefabricated angles are shown in Fig. 10. The permeability change characteristics in the triaxial test are divided into three types according to the experimental results.

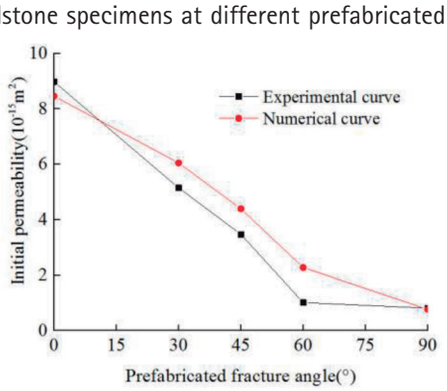

Fig. 9. The experimental and numerical values of the initial porosity of sandstone with infilled joint at different prefabricated angles

(1) When α=90° or 60°, the permeability curve is generally consistent with that of the intact sandstone specimen. Pore structures are closed under axial pressure and permeability decreases to a certain extent. The permeability of the specimens increases slightly during the linear elastic stage of deformation. With the gradual growth in external loads, microcracks first develop at joints when stress intensity reaches crack initiation stress. These microcracks serve as channels for fluid flow in the sandstone specimens. The growth rate of permeability is increased significantly. The maximum growth rate of permeability is achieved when stress intensity reaches damaging stress. During the post-peak stage, microcracks propagate and form the main crack zone along the prefabricated joint plane, which further increases permeability. Macroscopic shear failure occurs at the prefabricated joints, and the main crack zone is compacted by the compression effect. The growth rate of permeability decreases, and the specimens finally lose their bearing capacity. The failure mode indicates that the specimens are crushed severely and then became intact after losing their bearing capacity. Permeability increases significantly compared with initial permeability. The bond ruptures of particles are further developed into the secondary crack zone due to stress concentration on the macroscopic shear failure plane, which generate a large crack. This condition explains the sharp growth of permeability at the mesoscale. For example, the macroscopic shear failure at the prefabricated joint is caused by tensile cracks, which account for a high proportion of cracks when α=90°, as shown in Fig. 10(e). The secondary crack zone starts from one end of the joint and expands to the other end. It runs through the model boundaries with an increase in external load. The parallel bond is severely destroyed in the region outside from the joint shearing and secondary crack zone, and abundant nucleations of microcracks are increasingly formed and scattered. Seepage channels in the fluid domain, which are influenced by the nucleations of tensile cracks, increasing significantly along with internal porosity, as manifested by the overall growth of the permeability curve.

(2) When α=45° or 30°, the permeability–strain curve drops slightly during the early loading stage. Permeability increases rapidly during the early linear elastic stage of deformation. Then, it decreases slowly with an increase in axial pressure until the sandstone specimens finally fail. The failure mode indicates that jointed sandstone remains complete after the failure of the specimens. Therefore, permeability increases slightly compared with the initial permeability. For example, abundant shear cracks are developed at the prefabricated joint when α=45°, as shown in Fig. 10(c). Numerous microcracks are developed at the non-prefabricated area with an increase in steps, and shear cracks account for a high proportion. The permeability of the specimens achieves a sharp increase after the early decline, which is related to the low bond strength of the infilled joint. Many nucleations of shear cracks are formed under axial pressure and confining pressure. The infilled joint loses bearing capacity in advance. Dislocation slippage occurs between the upper and lower ends of the in-

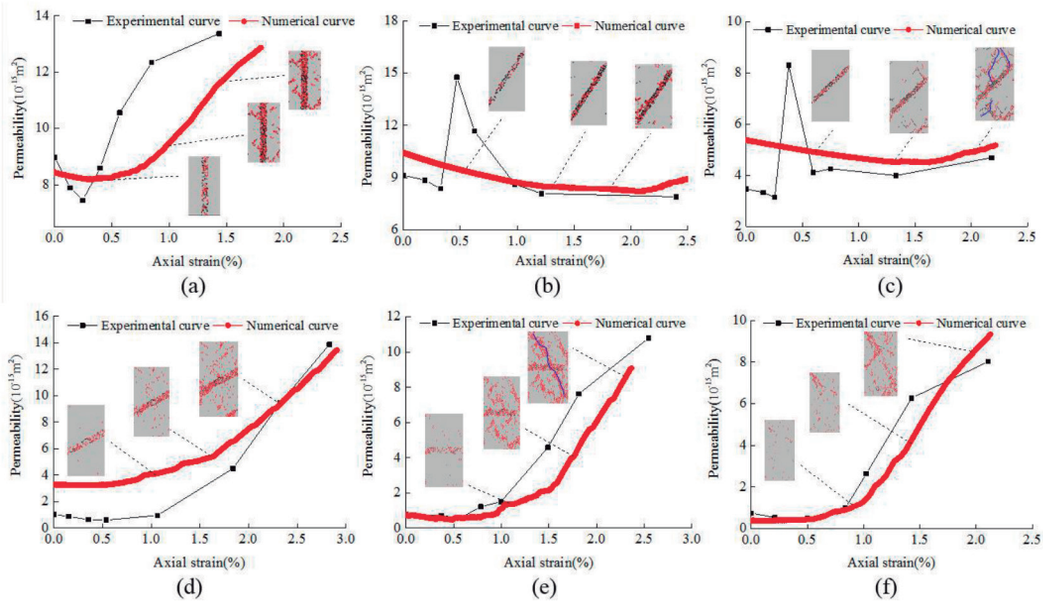

Fig. 10. Relation curves of the experimental and numerical permeability with strain at different prefabricated angles (a) α=0°. (b) α=30°.(c) α=45°.(d) α=60°.(e) α=90°.(f) Intact sample

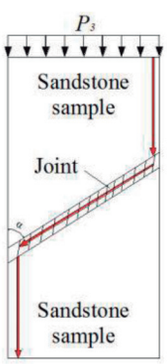

Fig. 11. The seepage principle process of sandstone with a single infilled joint

filled joint at two sides. Simultaneously, an interface fracture is developed along the infilled joint. Soft bonding particles are softened in water when osmotic pressure reaches the top of the infilled joint. Therefore, osmotic pressure can flow easily into the infilled joint. It flows out from the other end of the infilled joint and emanates from the bottom of the sandstone samples. Permeability rises to the peak value because the permeability of gypsum is two orders of magnitude higher than that of rocks. The seepage principle of the jointed sandstone is illustrated in Fig. 11 [19]. The infilled joint is fully compressed and the two cementing surfaces gradually approach each other with an increase in axial pressure. The sandstone specimen is further compacted. Moreover, the pores in rocks with low permeability replace the fillings in rocks with high permeability, which decreases permeability. The numerical simulation of permeability is mainly restricted by the mean particle size and mean porosity of the model. Therefore, the simulated curves of permeability are smooth, which fail to simulate the fluctuating curves in a triaxial test.

(3) The permeability at all the measuring points when α=0° is higher than that at other prefabricated angles given that the prefabricated joint lies along the axial direction of the specimens and that hydraulic pressure can be carried by the fillings from the upper position of the specimens to the lower end. Permeability declines slightly during the compaction stage. The bond between fillings and cementing surfaces are gradually weakened with a gradual increase in axial pressure until the bonding effect is finally lost. The specimens develop axial cracks along the prefabricated joint plane, and pore volume increases at the prefabricated joint. These conditions provide good channels for the longitudinal penetration of fluids and increase permeability. The numerical permeability curves exhibit a variation trend similar to that of the experimental curves. Permeability decreases gradually during the early loading stage. The proportions of tensile and shear cracks are generally equal at the abundant nucleations of microcracks in the specimens. The bond failure of particles increases pore volume among particles, which increases permeability.

5. CONCLUSION

The seepage failure of jointed rock has an important impact on geotechnical engineering practices. The mechanical properties and hydraulic properties of jointed rock directly affect the safety of engineering construction. Considering this point, it is necessary to clarify the seepage characteristics of joints in rock mass. Plenty of underground engineering and water conservancy projects often involve jointed rocks, revealing the law of seepage of jointed rocks is of great practical significance for the safety of mines, the stability of tunnel excavation, and prediction of groundwater movement. Therefore, it is of great significance to explore the mechanical properties and hydraulic properties of jointed rock.

The stress–seepage coupling test and the numerical simulation of jointed sandstone at the mesoscale at different prefabricated angles were analyzed comprehensively to discuss the triaxial compression mechanics and permeability evolution of sandstone with infilled joints under hydro-mechanical coupling conditions at different prefabricated angles. Several conclusions are drawn.

(1) Soft bonding particles can maintain strength stability under osmotic pressure during the post-peak stage. The peak strength of jointed sandstone is positively related to the bond strength of particles.

(2) The crack zone of jointed sandstone is mainly concentrated at the prefabricated joint. The integrity of sandstone after specimen failure influences the growth rate of permeability during the post-peak stage.

(3) The initial permeability of jointed sandstone decreases sharply at the radial distribution of soft bonding particles. The bond ruptures of particles cause tensile, shear, and secondary crack bands, which provide good channels for water penetration in jointed sandstone.

The constructed numerical model conforms to the laboratory test. The results of the numerical study are consistent with the experimental results and provide theoretical references for the study

the hydro-mechanical coupling effect of jointed sandstone at the mesoscale. However, several experimental phenomena are unexplainable at the mesoscale. The numerical model requires further improvement. In future studies, a series of expanded simulations will be conducted to interpret the mechanical properties and permeability evolution of jointed sandstone at the mesoscale under osmotic pressure–stress coupling conditions.

BIBLIOGRAPHY

[1] Fereidooni, D. "Influence of discontinuities and clay minerals in their filling materials on the instability of rock slopes". Geomechanics & Geoengineering. March 2017. Vol.1 p. 1-11. DOI: https://doi.org/10.1080/17486025.2017.1309080
[2] Zare, M. "Laboratory study of the shear behaviour of natural rough rock joints infilled by different soils". Periodica Polytechnica Civil Engineering. June 2015. Vol. 59-4. p. 431-421. DOI: https://doi.org/10.3311/PPci.7928
[3] Zhang W, Tang X Y, Weisbrod N, et al. "A coupled field study of subsurface fracture flow and colloid transport". Journal of Hydrology. May 2015. Vol. 524. p.476-488. DOI: https://doi.org/10.1016/j.jhydrol.2015.03.001
[4] Xiao T L, Li X P, Dai Y F. "Coupling analysis of seepage and stress in jointed rock mass of equivalent continuum". Advanced Materials Research. May 2011. Vol. 243-249. p.3493-3498. DOI: https://doi.org/10.4028/www.scientific.net/AMR.243-249.3493
[5] Fu P, Johnson S M, Carrigan C R. "An explicitly coupled hydro-geomechanical model for simulating hydraulic fracturing in arbitrary discrete fracture networks". International Journal for Numerical & Analytical Methods in Geomechanics. September 2013. Vol. 37-14. p.2278-2300. DOI: https://doi.org/10.1002/nag.2135
[6] Zhang L, Zhang J, Zhao Y. "Analysis of a finite element numerical solution for a nonlinear seepage flow model in a deformable dual media fractal reservoir". Journal of Petroleum Science & Engineering. March 2011. Vol. 76-3. p.77-84. DOI: https://doi.org/10.1016/j.petrol.2010.11.024
[7] Wong L N Y, Li D, Liu G. "Experimental studies on permeability of intact and singly jointed meta-Sedimentary rocks under confining pressure". Rock Mechanics & Rock Engineering. January 2013. Vol. 46-1. p.107-121. DOI: https://doi.org/10.1007/s00603-012-0251-0
[8] Wang H L, Xu W Y, Jia C J, et al. "Experimental research on permeabilityevolution with microcrack development in sandstone under different fluid pressures". Journal of Geotechnical & Geoenvironmental Engineering. June 2016. Vol. 142-6. p.0401-6014. DOI: https://doi.org/10.1061/(ASCE)GT.1943-5606.0001462
[9] Zhang Z, Nemcik J. "Fluid flow regimes and nonlinear flow characteristics in deformable rock fractures". Journal of Hydrology. January 2013. Vol. 477-1. p.139-151. DOI: https://doi.org/10.1016/j.jhydrol.2012.11.024
[10] Wang L, Liu J F, Pei J L, et al. "Mechanical and permeability characteristics of rock under hydro-mechanical coupling conditions". Environmental Earth Sciences. May 2015. Vol. 73-10. p.5987-5996. DOI: https://doi.org/10.1007/s12665-015-4190-4
[11] Wasantha P L P, Ranjith P G, Viete D R. "Comparative study of the hydromechanical behavior of intact, horizontally jointed, and vertically jointed rocks under undrained conditions". Journal of Materials in Civil Engineering. September 2016. Vol. 28-9. p.0401-6083. DOI: https://doi.org/10.1061/(ASCE)MT.1943-5533.0001591
[12] Wasantha P L P, Ranjith P G, Viete D R. "Effect of joint orientation on the hydromechanical behavior of singly jointed sandstone experiencing undrained loading". Journal of Geophysical Research Solid Earth. March 2014. Vol. 119-3. p.1701-1717. DOI: https://doi.org/10.1002/2013JB010600
[13] Li L C, Tang C A, Li G, et al. "Numerical simulation of 3D hydraulic fracturing based on an improved flow-stress-damage model and a parallel fem technique". Rock Mechanics & Rock Engineering. September 2012. Vol. 45-5. p.801-818. DOI: https://doi.org/10.1007/s00603-012-0252-z
[14] Shimizu H, Murata S, Ishida T. "The distinct element analysis for hydraulic fracturing in hard rock considering fluid viscosity and particle size distribution". International Journal of Rock Mechanics & Mining Sciences. July 2011. Vol. 48-5. p.712-727. DOI: https://doi.org/10.1016/j.ijrmms.2011.04.013
[15] Wang X G, Fu J W, Zhu W S, et al. "Numerical analysis on the failure process of jointed rock under the effect of seepage". Applied Mechanics & Materials. February 2014. Vol. 533. p.170-174. DOI: https://doi.org/10.4028/www.scientific.net/AMM.533.170
[16] Li L, Xia Y, Huang B, et al. "The behaviour of fracture growth in sedimentary rocks: a numerical study based on hydraulic fracturing processes". Energies. March 2016. Vol. 9-3. p.1-28. DOI: https://doi.org/10.3390/en9030169
[17] Marina S, Derek I, Mohamed P, et al. "Simulation of the hydraulic fracturing process of fractured rocks by the discrete element method". Environmental Earth Sciences. June 2015. Vol. 73-12. p.8451-8469. DOI: https://doi.org/10.1007/s12665-014-4005-z
[18] Yang T, Liu H Y, Tang C A, et al. "Scale effect in macroscopic permeability of jointed rock mass using a coupled stress–damage–flow method". Engineering Geology. October 2017. p.121-136. DOI: https://doi.org/10.1016/j.enggeo.2017.07.009
[19] Yu J, Chen X, Cai Y Y, et al. "Triaxial test research on mechanical properties and permeability of sandstone with a single joint filled with gypsum". Ksce Journal of Civil Engineering. September 2016. Vol. 20-6. p.2243-2252. DOI: https://doi.org/10.1007/s12205-015-1663-7
[20] Cheng C, Chen X, Zhang S. "Multi-peak deformation behavior of jointed rock mass under uniaxial compression: Insight from particle flow modeling". Engineering Geology. November 2016. Vol. 213. p.25-45. DOI: https://doi.org/10.1016/j.enggeo.2016.08.010
[21] Wang T, Zhou W, Chen J, et al. "Simulation of hydraulic fracturing using particle flow method and application in a coal mine". International Journal of Coal Geology. January 2014. Vol. 121. p.1-13. DOI: https://doi.org/10.1016/j.coal.2013.10.012
[22] Thornton C. "Granular dynamics, contact mechanics and particle system simulations". Springer International Publishing. January 2015. DOI: https://doi.org/10.1007/978-3-319-18711-2
[23] Izmailov V V. "Calculation of characteristics of discrete adhesive contact". Journal of Friction & Wear. September 2014. Vol. 35-5. p.343-350. DOI: http://dx.doi.org/10.3103/S1068366614050079
[24] Nooruddin H A, Hossain M E. "Modified kozeny–carmen correlation for enhanced hydraulic flow unit characterization". Journal of Petroleum Science & Engineering. December 2011. Vol. 80-1. p.107-115. DOI: https://doi.org/10.1016/j.petrol.2011.11.003

APPRECIATION

This study was supported by National Natural Science Foundation of China (51679093 and 51774147), Open Research Fund of State Key Laboratory for Geomechanics and Deep Underground Engineering, China University of Mining and Technology, China (SKLGDUEK1701), Program for New Century Excellent Talents in Fujian Province University, China, Natural Science Foundation of Fujian Province of China (2017J01094), and Promotion Program for Young and Middle-aged Teacher in Science and Technology Research of Huaqiao University (ZQN-PY112 and ZQN-PY311), China.

SUPPLEMENTARY MATERIAL

https://www.revistadyna.com/documentos/pdfs/_adic/8757-1.pdf